Hindawi
Journal of Advanced Transportation
Volume 2018, Article ID 8103140, 14 pages
https://doi.org/10.1155/2018/8103140

Research Article

Application of Wireless Power Transfer to Railway Parking Functionality: Preliminary Design Considerations with Series-Series and LCC Topologies

Luca Pugi,[1] **Alberto Reatti**,[2] **and Fabio Corti**[2]

[1]*DIEF (Industrial Engineering Department), University of Florence, Via di Santa Marta 3, 50139 Firenze, Italy*
[2]*DINFO (Department of Information Engineering), University of Florence, Via di Santa Marta 3, 50139 Firenze, Italy*

Correspondence should be addressed to Luca Pugi; luca.pugi@unifi.it

Received 27 August 2018; Accepted 6 December 2018; Published 27 December 2018

Guest Editor: Stefano Bracco

There is a wide literature concerning the application of inductive power transfer (IPT) to light railway systems. In this work, proposed application is innovative with respect to existing literature: static current collection on conventional railway lines is proposed in order to replace the functionalities implemented by conventional battery chargers and the so-called railway "parking" system. According to standards in force, current collection in standstill conditions is limited since pantograph contact shoes and catenary wires have to be protected by thermal overload. These limitations have to be considered since power demand for all the services installed on modern coaches should be higher than 20-40kW. This is a critical technical issue especially for long compositions that have to be prepared for service by activating on-board subsystems such as heating and air conditioning. Additional possible applications should be related to refrigerated wagons in freight compositions. In all these cases the availability of a simple, safe, and compact system should be useful to ensure a wireless power collection to on-board equipment. In this work authors introduce the proposed application and perform some preliminary design considerations. With respect to current literature on IPT systems, authors also introduce some innovative design criteria based on the analogy between resonant electrical system and corresponding mechanical ones. In this way, sizing of the proposed IPT system can be performed using modal methods that are also used for the proper sizing of mechanical vibrating systems, such as example, vehicle suspensions, or pantograph systems.

1. Introduction: The Proposed Application Of Inductive Wireless Power Transfer

There is a big interest in the development of wireless power transfer system for tramways, light trains, and cars in order to eliminate encumbrances and risk connected to the usage of electrified catenaries in urban environment [1].

One example is the Primove™ system developed by Bombardier [2]. IPT systems (inductive power transfer) have been also proposed for Maglev trains where the high speed makes the current collection through a sliding contact difficult [3, 4].

In this work, authors consider a different application: the usage of IPT system for static recharge of railway batteries and more generally to feed on-board subsystems in standstill conditions. Proposed application is innovative: this specific application for conventional railways is not currently considered in literature.

This solution is proposed in order to avoid a prolonged static current collection that should be difficult to be managed: in standstill conditions currents have to be limited mainly to avoid thermal overload of the electric contact interface between pantograph and catenary.

These limitations are mainly due to thermal troubles: in standstill conditions all the power is collected on a fixed limited area (1-2cm^2) since contact geometry is fixed and cooling is not available [5].

Current limits defined with respect to considered overhead lines and specific electrification standards [6, 7] are shown in Table 1: especially on DC lines, prescribed current limitations correspond to relatively small collected powers.

Table 1: Current limitation in standstill conditions according to regulations in force [6, 7].

Voltage Level	1.5 kV DC	3 kV DC	25 kV 50 Hz AC	15 kV 16&2/3Hz AC
Current Level	300 [A]	200[A]	80 [A]	80 [A]
Corresponding Nom. Power Limit	450[kW]	600[kW]	2[MW] (max power factor)	1.2[MW] (max power factor)

(a) E464 locomotive in parking mode

(b) ETR 500 in standstill solution [7]

Figure 1: Examples of trains in parking conditions.

Auxiliary services on each coach correspond to a continuous mean load of at least 20-40 kW.

Examples of fundamental on-board services are the following ones: Heating-Air Conditioning, Lights/Illumination, access management (doors), and finally the recharge of on-board accumulators.

Also brake compressors for pneumatic services involve an additional peak consumption of 200-400 kW: pneumatic systems are an important source of consumptions, since pneumatic suspensions, brake plants, and other on-board actuations have to be pressurized and ready even when the train is in standstill condition.

As a consequence, for a standard composition of 10-12 coaches, power consumptions have to be monitored and limited in order to respect prescribed current limits.

This monitoring is very important especially when an unmanned management of the train is prescribed.

An example in this sense is the so-called "parking mode": "parking" is a functionality that allows an unmanned activation of current collection from catenary while the train is in standstill conditions. Aim of this functionality is to prepare or maintain a train ready for service without the presence of the human driver. This is very useful since allowing speeding up the preparation of the train, recharging batteries, maintaining internal comfort acceptable, and keeping alive fundamental services such as lights, doors, etc.

"Parking" is the name of the functionality which is mostly used in Italy; however similar systems are finding an increasing diffusion among different countries and railway administrations.

As visible in Figure 1, when parking functionality is activated, pantograph is lifted up to collect current and red lights are switched in order to inform that unmanned control of on-board power system is working.

The application to monitored parking functionalities is only an example of possible uses of static inductive power transfer systems which authors consider confined to recharge of on-board subsystems: recent studies [8] have demonstrated that also for high speed trains systems efficiency of conventional power collection with catenary is high and it can be increased by further exploiting regenerative braking.

Figure 2 shows a simplified scheme of the proposed system: a primary inductor fixed to the ground excites a receiver pad/coil installed on the vehicle: pads are coupled through electromagnetic flux linkages.

Power transmitted to receiver pad is used to recharge on-board batteries and more generally to feed a DC power bus along the train.

There is a wide literature [9–11], regarding wireless power transfer systems; however, authors proposed an original approach based on a multiphysic analogy between resonant electrical system and mechanical vibrating ones [12].

Proposed approach is described in detail in the following section: the electrical system is converted in an equivalent mechanical one demonstrating that the optimization of an IPT should be treated as the one of an equivalent mechanical suspension system.

In this way, tuning of resonant circuits can be performed using interdisciplinary techniques also known by mechanical and railway engineers (vibration control is a common topic for vehicle engineering).

2. Preliminary System Specifications

Table 2 shows some specifications for the proposed system: it is considered a single phase pad feed by DC current obtained by rectifying an industrial three-phase source; current proposal admits a large space availability under car

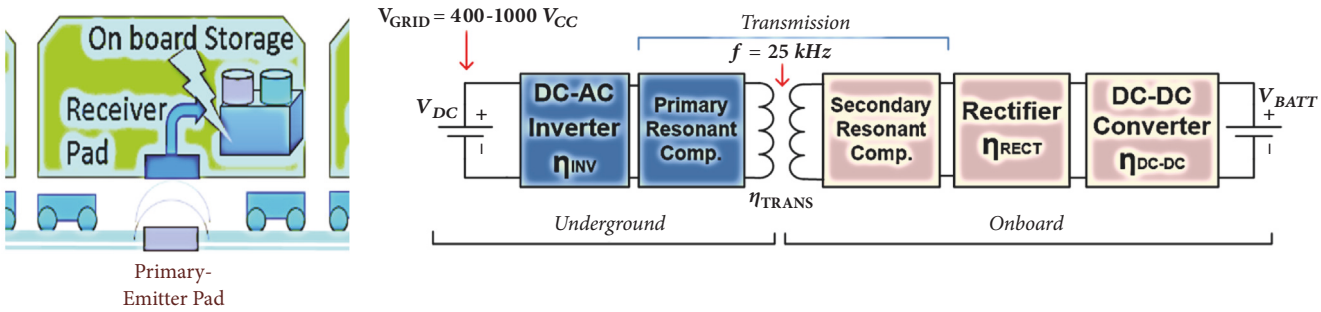

Figure 2: Proposed wireless, static recharge system.

Table 2: Proposed system characteristics.

Parameter	Value	Description
S_{PAD}	1 [m^2]	PAD Surface
z	0.85 [m]	Airgap
P_{out_max}	20-30 [kW]	Maximum Output Power
P_{out_typ}	10-15[kW]	Typical Output Power
V_{out}	400-1000 [V]	Output Voltage
V_{in_CC}	565.7[V] ∗	Input Voltage
f_s	25 [kHz]	Switching Frequency

∗Authors supposed to use a connection to the industrial three-phase line to produce the rectified input voltage used to fed the inverter of the primary coil.

body corresponding to a max encumbrance of about 1-1.1 meter resulting in an admissible pad area of about 1m^2.

Large encumbrances of the pad have been preferred (a more compact design is clearly possible) for the following reasons:

(i) Large air-gap is also specified (0.85m).

(ii) A low sensitivity with respect to relative positioning of pads should be appreciated.

(iii) System can be easily upgraded to higher power transfer for future, more demanding applications.

(iv) Required encumbrances are not so demanding for a railway systems; a relatively low power density should help to improve system resilience against harsh specifications of railway environment in terms of operating temperatures avoiding any additional cooling system.

Obviously by relaxing overcited specifications, a high optimization in terms of encumbrances is feasible (this is only a preliminary study).

For design, a continuous power transfer of 15 kW and a peak power of 20-30 kW are considered feasible specifications to recharge a single coach.

Working voltages of railway accumulators are typically quite low (24 V-120 V); however it should be considered the necessity of feeding common DC bus with voltages between 400V (as in ETR500 Italian high speed train) and 1000V: this voltage range is the more diffused since vehicle DC bus has to feed inverters for three-phase loads like motors of pneumatic compressors or pumping units of air-conditioning systems.

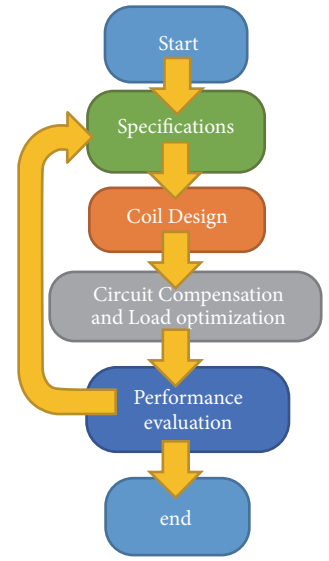

Figure 3: Adopted design process.

All these systems are typically associated with high power requirements.

3. Proposed Design Procedure

Starting from specifications described in Section II, authors performed a preliminary design according to the procedure shown in Figure 3:

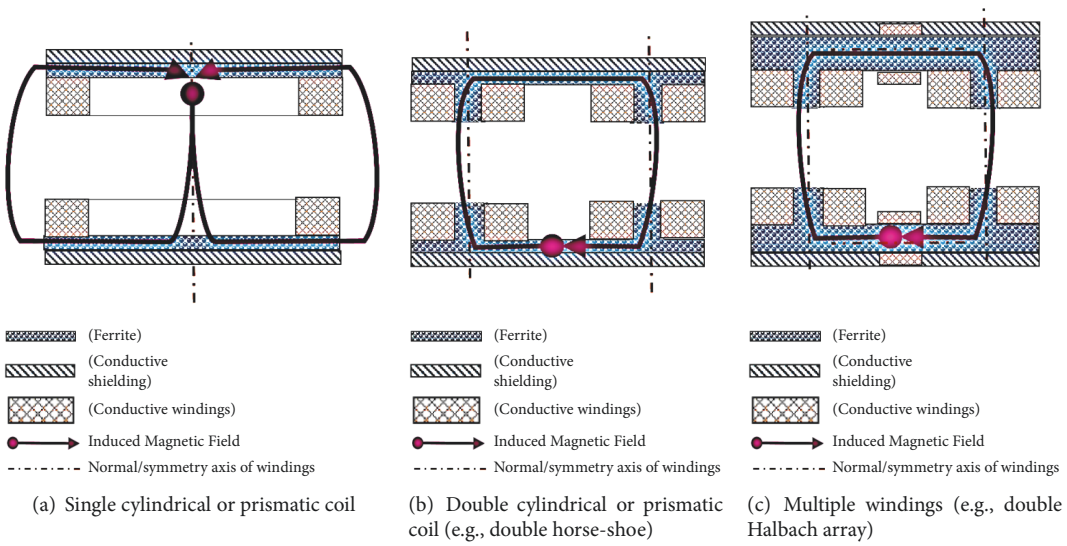

(a) Single cylindrical or prismatic coil

(b) Double cylindrical or prismatic coil (e.g., double horse-shoe)

(c) Multiple windings (e.g., double Halbach array)

Figure 4: Examples of single phase, planar pads used for inductive power transfer.

(i) Design of coil pads ("Coil Design" phase): coil geometry, including conductive sections.

(ii) Pad compensation: both pads are connected to resonant circuits that have to be optimized; two different topologies are investigated, the series-series one and LCC.

(iii) System performances are simulated; these results are evaluated suggesting modifications and further design optimizations; in this work intermediated iterations are not described.

4. Coil Design

For the proposed application, single or three-phase coils should be considered: in this work authors started from single phase coils.

An equivalent three-phase design should be the object of a further system optimization once its feasibility is demonstrated.

For single phase pads, different shapes and layout are discussed in literature [9–11]: some examples are shown in Figures 4(a), 4(b) and 4(c).

In this work authors have considered the simplest geometry, visible in Figure 4(a): a single axial symmetric, circular coil.

Chosen layout is less efficient (in terms of electromagnetic coupling) with respect to other ones described in Figures 4(b) and 4(c) but much simpler in terms of optimization and prototyping. This is a high desirable feature, especially for the construction of a prototype for experimental activities (future step of the research activity). In this sense the chosen design for the prototype is cautious with respect to the final fully optimized industrial product.

Coils have to be fed at 25 KHz, so use of Litz wires is highly recommended in order to optimize conductive sections with respect to undesired "skin effect" that should penalize a solid conductor with respect to a multistrand one. A Litz wire consists of many strands, individually insulated and twisted, often involving bundles.

The first step for designing a Litz wire is to find the copper size, usually defined from the American wire gauge (AWG).

AWG size has to be optimized with respect to conduced current. Assuming a good efficiency η (η_{TRASM} approximately equal to 0.9), maximum input current on the primary coil I_{in} is calculated according to

$$I_1 = \frac{P_{out}}{\eta V_{ac}} \tag{1}$$

Optimal strand diameter is chosen according to working frequency: depth of induced conductive skin is substantially insensitive with respect to wire size: a wire radius comparable to induced conductive skin is considered an optimal solution.

For a working frequency of 25kHz, an AWG36 (d= 0.127 mm) is a good choice.

Figure 5 shows some simulation results (FEM Simulations performed by authors with Comsol Multiphisic™): a straight copper solid wire is simulated imposing a forced voltage input; a frequency response simulation is performed; a very fine mesh is needed since the size of the mesh should be much lower with respect to simulated skin depth (ideally at least a magnitude lower).

Current density in single strands with different diameters is shown: skin effect is clear noticeable for strands with higher diameters with respect to nominal one.

Knowing the suggested current for each strand ($I_{\max\_strand}$), the minimum number of wire strands $N_{strands\_min}$ is calculated according to

$$N_{strands\_\min} = \frac{I_1}{I_{\max\_strand}} \tag{2}$$

External diameter of the coil is constrained by encumbrance specifications. For pad design, authors have considered a

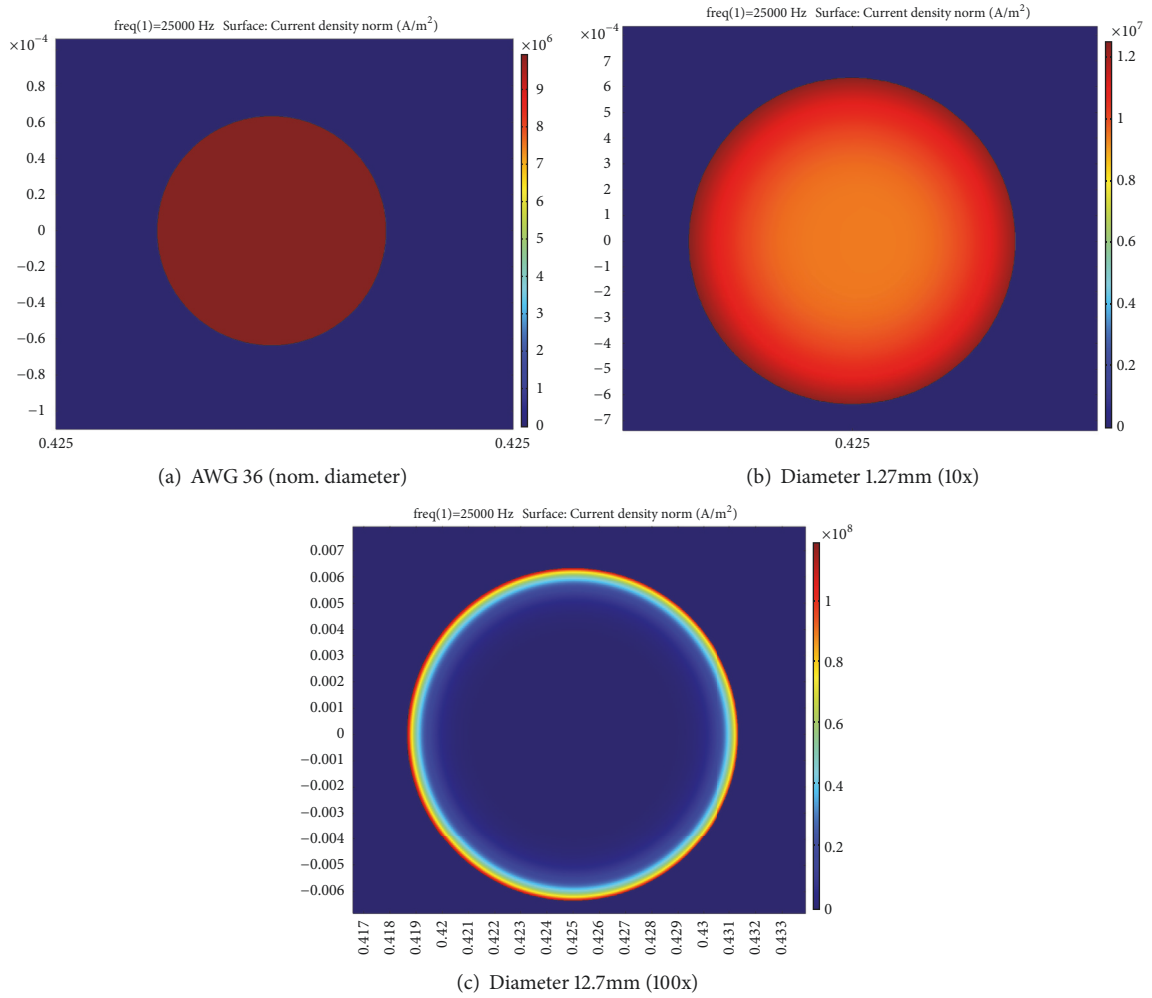

(a) AWG 36 (nom. diameter)

(b) Diameter 1.27mm (10x)

(c) Diameter 12.7mm (100x)

Figure 5: Current density of single strand wires fed at a 25 KHz, comparison between different diameters (FEM simulations performed with Comsol Multiphisics™).

Table 3: Proposed coils parameters.

Parameter	Value	Description
N	53	Number of Turns
w	5.19 [mm]	Wire Diameter
D_o	1.128 [m]	Outer Diameter
D_i	0.05 [m]	Inner Diameter
d	0.005 [m]	Distance between Turns
L	1.084 [mH]	Wheeler Inductance
R_{Wojda}	0.358[Ω]	Coil Resistance Calculated according [11]

single planar layer described in Figure 6. For the considered coil, it is possible to calculate inductance using Wheeler relationships [10].

Also to evaluate coil resistance, there are some suggested relationships in literature [14, 15]. Precision of these relations have been widely studied and verified by authors using Finite Elements Models [16]. Authors preferred over-cited relations to perform an iterative design since their usage is still much faster with respect to FEM models.

Finally, it should be noticed from results shown in Figure 5, that, for an operating frequency of 25kHz, skin effect on an AWG 36 strand is almost negligible: resistance of the wire (at 25 kHz) is almost equal to the static value calculated with the standard Ohm law.

In Table 3 some parameters of the proposed coil are shown (both pads are supposed to have the same coil).

Mutual inductance M_{12} between coils is calculated according to relation (3), proposed by Raju et al. [17].

$$M_{12} = \rho \sum_{i=1}^{n_p} \sum_{j=1}^{n_s} L_{m\_ij} \tag{3}$$

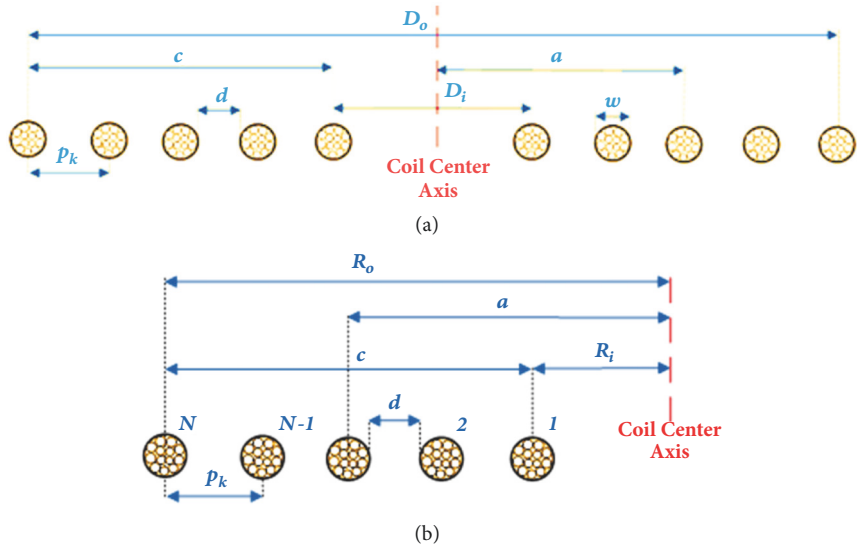

Figure 6: Coil cross-section, entire one (a) and half one (b).

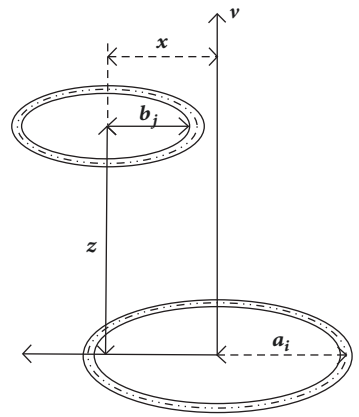

Figure 7: Scheme adopted to calculate self-inductance and mutual inductances of coils.

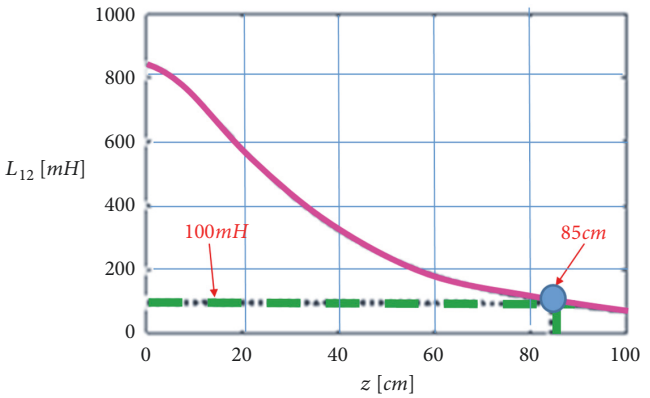

Figure 8: Calculated behavior for mutual impedance of coils with respect to air-gap.

n_P and n_S are the number of turns for the primary and secondary inductors, respectively.

Parameter ρ depends on the shape of the planar coils. If both the primary and secondary planar coils are circular shaped, $\rho = 1$.

In relation (3), following variables are introduced (see coil schemes of Figures 6 and 7):

$$L_{m\_ij} = \frac{\mu_0 \pi a_i^2 b_i^2}{2\left(a_i^2 + b_i^2 + z^2\right)^{3/2}} \left(1 + \frac{15}{32}\gamma_{ij}^2 + \frac{315}{1024}\gamma_{ij}^4\right)$$
$$\gamma_{ij} = \frac{2a_i b_j}{\left(a_i^2 + b_j^2 + z^2\right)} \quad (4)$$

Considering an air-gap value z of 0.85 m, calculated mutual inductance is approximately equal to 100 μH, and corresponding value of coupling coefficient k is equal to 0.1, as visible in Figure 8.

5. Optimization of Load and Circuit Compensation

As stated by works in literature inductive pads are weakly coupled in air (low values of k, mutual inductance merit factor).

To improve power transfer between pads, both coils are compensated using capacities producing a resonant system.

Different compensation topologies are suggested in literature [13, 18].

In this work authors considered two of the most commonly used configurations for vehicle systems: series-series and LCC [19] compensations: corresponding circuits are visible in Figure 9.

Looking at Figures 9(a) and 9(b), LCC topology should be considered as a further development of series-series one: on both circuits resonant LC branches are added.

In literature [13, 18, 19], design and optimization methods for both topologies are presented.

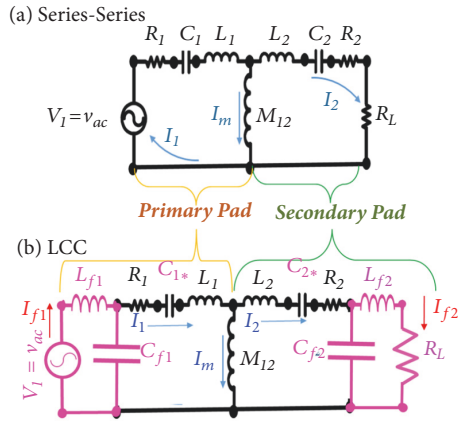

Figure 9: Series-series (a) and LCC (b) compensation topologies.

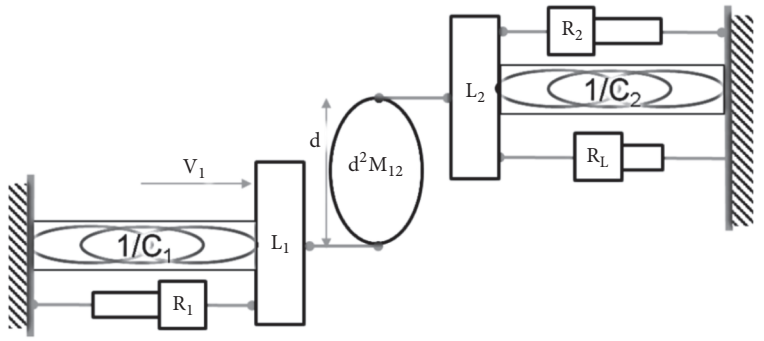

Figure 10: Equivalent 2-DOF mechanical system (series-series topology).

Table 4: Equivalence between magnetic and electric systems [13].

Domain	Generalized Flow	Generalized Effort	Generalized Displacement	Resistance	Inertance	Compliance
Mechanical-Linear	Speed v	Force F	Displ. x	Damping D	Mass M	Compl. $1/K$
Mechanical-Rotational	Speed ω	Torque T	Angle α	Ang.Damp. D_t	Inertia J	Compl. $1/K_t$
Electrical	Current I	Voltage V	Charge q	Resistance R	Inductance L	Cap. C

In particular, there is an increasing interest for the LCC topology especially on recent publications [20–22].

However, authors preferred to apply their own innovative approach: exploiting the electromechanical analogy proposed by Karnopp [23, 24], it is possible to model electric resonant circuits as equivalent vibrating mechanical systems.

In this way, a consolidated know-how concerning modal analysis of mechanical systems [25–27] can be exploited.

Proposed electromechanical equivalence is described in Table 4.

5.1. Compensation of Series-Series Topology. Electromechanical analogy described in Table 4 is applied to series-series topology described in Figure 9(a).

The equivalent mechanical system is described in Figure 10: inductances are equivalent to inertial terms, capacities to spring elements, resistors to dampers; displacements of the mechanical system are equivalent to corresponding charges q_1, q_2 stored on capacitors (C_1, C_2).

Optimization of the topology can be treated as an equivalent mechanical problem: power transmitted to equivalent damper R_L (load resistance) has to be optimized.

Dynamical behavior of the system described in Figure 10 is represented by (5); Mass, Damping, and Stiffness matrices are defined, respectively, as M, D, K.

$$M\ddot{x} + D\dot{x} + Kx = F$$

$$x = \begin{bmatrix} q_1 \\ q_2 \end{bmatrix};$$

$$F = \begin{bmatrix} V_1 \\ 0 \end{bmatrix};$$

$$M = \begin{bmatrix} L_1 + M_{12} & -M_{12} \\ -M_{12} & L_2 + M_{12} \end{bmatrix};$$

$$D = \begin{bmatrix} R_1 & 0 \\ 0 & R_2 + R_L \end{bmatrix};$$

$$K = \begin{bmatrix} \frac{1}{C_1} & 0 \\ 0 & \frac{1}{C_2} \end{bmatrix} \tag{5}$$

Electrical resonating systems are weakly damped since resistances on coils are usually minimized in order to reduce internal losses.

R_L is applied only on secondary coil, so the hypothesis of proportional damping is not exactly verified: according to Ewins [25] damping is proportional when matrix D can expressed as a linear combination of matrices M (inertial terms) and K (elastic terms). However, for weakly damped systems, the hypothesis of proportional damping can be applied approximately producing negligible errors.

Also, for the proposed application, primary and secondary coils are equals (R_1=R_2; $L_1 = L_2$).

Damping matrix D is decomposed according to (6) in two contributions D_P and D_N:

$$D = \begin{bmatrix} R_1 & 0 \\ 0 & R_2 + R_L \end{bmatrix} \overbrace{=}^{R_1=R_2} \begin{bmatrix} R_1 & 0 \\ 0 & R_1 + R_L \end{bmatrix}$$

$$= \overbrace{\begin{bmatrix} R_1 + \frac{R_L}{2} & 0 \\ 0 & R_1 + \frac{R_L}{2} \end{bmatrix}}^{D_P} + \overbrace{\begin{bmatrix} -\frac{R_L}{2} & 0 \\ 0 & \frac{R_L}{2} \end{bmatrix}}^{D_N} \tag{6}$$

The system is studied as an approximated proportional one, where contribution of nonproportional terms (matrix D_n) is neglected.

According to over-cited hypothesis, maximum efficiency in power transfer is obtained when the system is excited with an optimal input frequency ω_{opt} (7).

$$\omega_{opt} = \sqrt{\frac{1}{C_1 L_a}} \tag{7}$$

L_a, the total inductance of the coil, is defined according to

$$L_a = \overbrace{M_{12}}^{\substack{\text{mutual} \\ \text{inductance}}} + \overbrace{L_1}^{\substack{\text{disp.} \\ \text{induct.}}} = L_b = \overbrace{M_{12}}^{\substack{\text{mutual} \\ \text{inductance}}} + \overbrace{L_2}^{\substack{\text{disp.} \\ \text{induct.}}}; \tag{8}$$

Mutual (M_{12}) and dispersed ($L_1 = L_2$) inductances are calculated from the definition of the merit factor k_m(9):

$$k_m = \frac{M_{12}}{\sqrt{L_a L_b}} \quad if\ (L_a = L_b) \Longrightarrow$$

$$k_m = \frac{M_{12}}{L_a} = \frac{M_{12}}{(M_{12} + L_1)}; \tag{9}$$

Optimal value of the compensating capacitors (10) is calculated from (8) since both L_a and ω_{opt} are known:

$$C_1 = C_2 = \frac{1}{\omega_{opt}^2 L_a} \tag{10}$$

R_{opt} is the optimal value of R_L that maximize efficiency. Optimal efficiency is verified when the weighted damping coefficient k_ε (11) has a unitary value.

$$k_\varepsilon \approx \frac{\xi_1 \omega_{n1*} + \xi_2 \omega_{n2*}}{\omega_{n2*} - \omega_{n1*}}$$

$$\approx \frac{2\left(R_1 + R_L/2\right)}{\sqrt{\left(L_a/C_1\right)\left(1 - k_m^2\right)}\left(\sqrt{1 + k_m} - \sqrt{1 - k_m}\right)} \approx 1 \tag{11}$$

k_ε is defined as a function of modal damping coefficients ξ_1, ξ_2 (12) and corresponding natural frequencies ω_{n1*}, ω_{n2*} (13).

$$\xi_1 = \frac{R_1 + R_L/2}{\sqrt{L_a\left(1 + k_m\right)/C_1}};$$

$$\xi_2 = \frac{R_1 + R_L/2}{\sqrt{L_a\left(1 - k_m\right)/C_1}}; \tag{12}$$

$$\omega_{n1^*} = j\sqrt{\frac{1}{2C_1 M_{12} + C_1 L_1}} = j\sqrt{\frac{1}{C_1 L_a\left(1 + k_m\right)}};$$

$$\omega_{n2^*} = j\sqrt{\frac{1}{C_1 L_1}} = j\sqrt{\frac{1}{C_1 L_a\left(1 - k_m\right)}}; \tag{13}$$

Optimization procedure above described is performed on an approximated system with proportional damping.

In order to verify the behavior of the proposed optimization, some numerical simulations are performed on an exact model in which over-cited simplifications are not applied (full damping matrix D is applied, without considering the approximating assumption of proportional damping). The numerical model is developed using Matlab-Simulink™.

Some results are shown in Figures 11 and 12.

Behavior of efficiency η with respect to both frequency and k_ξ is shown in Figure 11: optimal efficiency is substantially reached in the same conditions (unitary value of k_ξ and frequency equal to ω_{opt}) prescribed by the approximated model with proportional damping. In nominal conditions transferred power is about 15 kW with efficiency of about 95-96%.

In order to increase transfer rate of the system to 30 kW, output load R_L should be increased in order to obtain a higher value of k_ξ that is doubled with respect to the optimum one (R_{opt}).

In this condition, also the value of K_ξ is doubled (K_ξ=2), but efficiency is still very high (about 94-95%).

As a consequence, power transfer should be modulated with limited consequences on efficiency.

High efficiency involves limited losses (about 1.5 kW with a 30 kW of transferred power): considering coil dimensions,

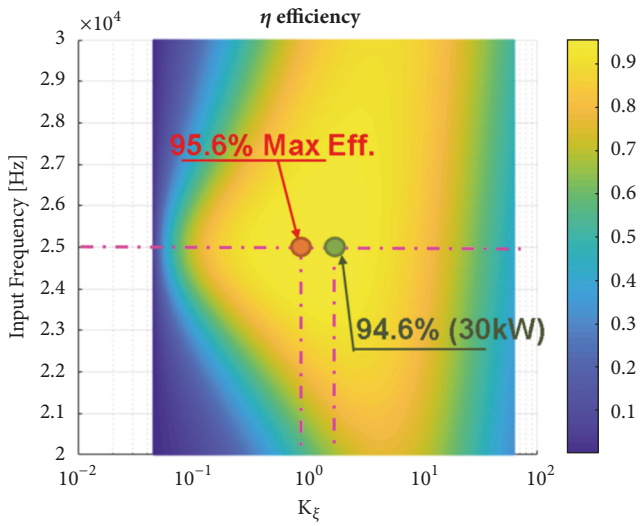

Figure 11: Efficiency of the proposed solution with respect to input frequency and k_ξ.

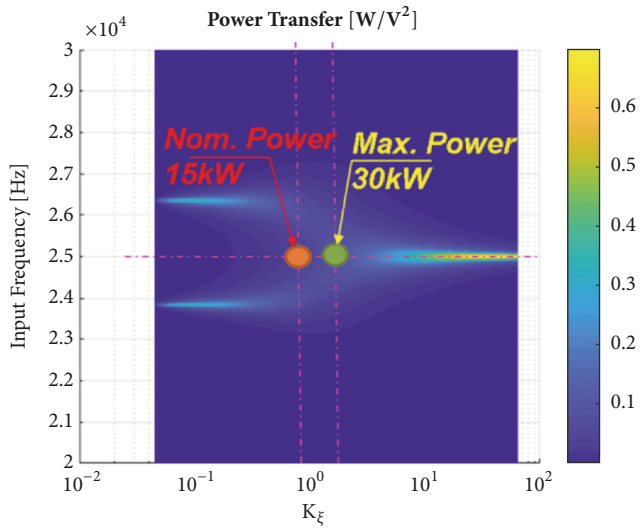

Figure 12: Different working conditions of the proposed equipment.

these losses can be easily managed without the need of additional cooling systems. So, with a proper cooling, the system can be further overloaded.

Figure 12 shows the behavior of transferred power scaled with respect to the squared value of input voltage.

Chosen operating conditions corresponds to a relatively low value of transferred power with respect to input voltage.

However, it should be noticed that transferred power depends from the squared value of input voltage.

As a consequence, a limited increase of the input voltage produces a high increase of transferred power.

Features of the proposed series-series compensation are quite interesting.

However, there is an important drawback: performances are constrained to a very precise value of load resistance.

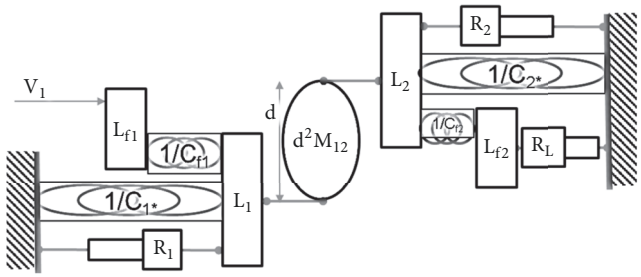

Figure 13: Equivalent 4-DOF mechanical system for the LCC topology.

A proper load matching should be performed adopting a transformer or a static converter such as a controlled rectifier.

These additional components introduce further costs and losses, penalizing the system.

5.2. Compensation of the LCC Topology. Optimization of series-series compensation involves a precise value of load resistance R_L that should be equal to a corresponding optimal value R_{opt} calculated imposing a near to unitary value of K_ξ.

LCC topology should be a valid solution to optimize optimal load matching with the introduction of a limited number of simple passive components.

The equivalent mechanical system for LCC topology is represented in Figure 13: an additional degree of freedom is introduced on both coils to model additional inductive and capacitive elements; resulting system has four degree of freedom.

Dynamical behavior of the system shown in Figure 13 is described by

$$M\ddot{x} + D\dot{x} + Kx = F$$

$$M = \begin{bmatrix} L_{f1} & 0 & 0 & 0 \\ 0 & L_1 + L_m & -L_m & 0 \\ 0 & -L_m & L_2 + L_m & 0 \\ 0 & 0 & 0 & L_{f2} \end{bmatrix};$$

$$D = \begin{bmatrix} 0 & 0 & 0 & 0 \\ 0 & R_1 & 0 & 0 \\ 0 & 0 & R_2 & 0 \\ 0 & 0 & 0 & R_L \end{bmatrix};$$

$$K = \begin{bmatrix} \frac{1}{C_{f1}} & -\frac{1}{C_{f1}} & 0 & 0 \\ -\frac{1}{C_{f1}} & \frac{1}{C_{f1}} + \frac{1}{C_{1*}} & 0 & 0 \\ 0 & 0 & \frac{1}{C_{f2}} + \frac{1}{C_{2*}} & -\frac{1}{C_{f2}} \\ 0 & 0 & -\frac{1}{C_{f2}} & \frac{1}{C_{f2}} \end{bmatrix};$$

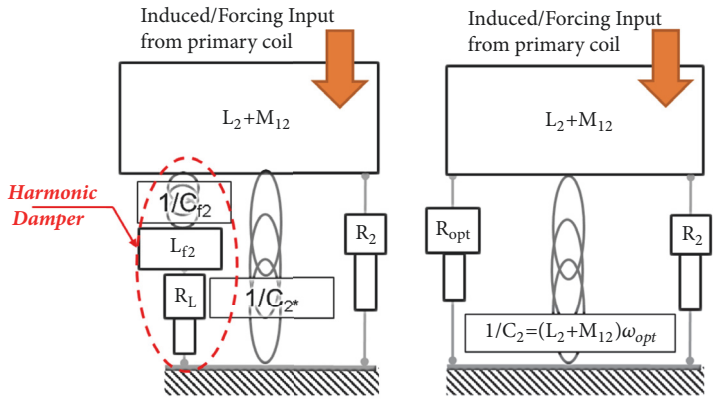

Figure 14: Equivalent 2DOF model of the secondary pad of the LCC compensation (a) and series-series circuit that has to be emulated (b).

$$x = \begin{bmatrix} q_{f1} \\ q_1 \\ q_2 \\ q_{f2} \end{bmatrix}; \quad F = \begin{bmatrix} 0 \\ V_1 \\ 0 \\ 0 \end{bmatrix}; \tag{14}$$

Each circuit (primary and secondary) is optimized by imposing the equivalence between mechanical impedance of series-series topology and LCC one.

In particular, L_{f2} and C_{f2} are optimized considering the two degree of freedom models of Figure 13: the system can be studied as a particular case of harmonic damper [28, 29] which is a common technical problem for mechanical engineers.

L_{f2} and C_{f2} have to be tuned in order to emulate the behavior of the optimal impedance of the series-series compensation layout at input frequency ω_{opt}.

In this way the study is treated as a classical problem of emulation of mechanical impedance: this is also a typical topic for mechanical engineers dealing with the optimization of suspension systems, such as example, the ones of a railway pantographs [4].

In order to properly design the system, the harmonic damper (Figure 14(a)) has to resonate at frequency ω_{opt}, so relation (15) has to be verified:

$$\omega_{opt}^2 = \frac{1}{C_{f2}L_{f2}} \Longrightarrow \quad C_{f2} = \frac{1}{L_{f2}\omega_{opt}^2} \tag{15}$$

Lumped elements of the harmonic damper are connected in series, so also relation (16) has to be verified.

$$-\omega_{opt}^2 L_{f2} q_{f2} + jR_L\omega_{opt}q_{f2} + \underbrace{\frac{1}{C_{f2}}}_{\omega_{opt}^2 L_{f2}}\left(q_{f2} - q_2\right) = 0 \Longrightarrow \quad q_2 = j\frac{R_L}{\omega_{opt}L_{f2}}q_{f2} \tag{16}$$

Equivalent impedance of the two systems has to be equal (17):

$$\frac{1}{C_{f2}}\left(q_2 - q_{f2}\right) + \frac{1}{C_{2*}}q_2 = \frac{1}{C_2}q_2 + j\omega_{opt}R_{opt}q_2 \tag{17}$$

Merging relation (17) with (16) and (15) relation (18) is calculated:

$$-q_{f2}L_{f2}\omega_{opt}^2 = j\frac{R_L}{\omega_{opt}L_{f2}} \cdot q_{f2}\left(j\omega_{opt}R_{opt} + \left(M_{12} + L_2 - L_{f2}\right)\omega_{opt}^2 - \frac{1}{C_{2*}}\right) \tag{18}$$

Solving (18), optimal values of C_{2*} (19) and L_{f2} (20) are evaluated.

$$\left(M_{12} + L_2 - L_{f2}\right)\omega_{opt}^2 - \frac{1}{C_{2*}} = 0 \Longrightarrow \quad C_{2*} = \frac{1}{\left(M_{12} + L_2 - L_{f2}\right)\omega_{opt}^2} \tag{19}$$

$$L_{f2}\omega_{opt}^2 = \frac{R_L R_{opt}}{L_{f2}} \Longrightarrow \quad L_{f2} = \frac{\sqrt{R_L R_{opt}}}{\omega_{opt}} \tag{20}$$

Table 5: Parameters of the simulated circuit with LCC compensation.

Parameter	Value	Parameter	Value
L_{f1}	9.74e-05[H]	L_{f2}	9.74e-05[H]
L_1	9.16e-04[H]	L_2	9.16e-04[H]
M_{12}	1.018e-04[H]	$R_L = R_{opt}$	15.3[Ω]
C_{f1}	4.161e-07[C]	C_{f2}	4.161e-07[C]
C_{1*}	4.40e-08 [C]	C_{2*}	4.40e-08 [C]

For primary coil the same sizing principles are followed, so it is possible to define, respectively, L_{f1} (21), C_{f1} (22), and C_{1*}(23):

$$L_{f1} = \frac{\sqrt{(V_1/I_1)\,R_{opt}}}{\omega_{opt}} \tag{21}$$

$$C_{f1} = \frac{1}{L_{f1}\omega_{opt}^2} \tag{22}$$

$$C_{1*} = \frac{1}{\left(M_{12} + L_1 - L_{f1}\right)\omega_{opt}^2} \tag{23}$$

From above described relations it should be easily argued the main advantage of LCC compensation with respect to series-series one: system can be designed for values of R_L that are quite different with respect to R_{opt} using only passive components.

5.3. Simulation Results for LCC Topology. In order to verify performances of LCC compensation, authors performed some simulations with a full Matlab-Simscape™ model of the circuit whose main parameters are described in Table 5. The model is composed by standard lumped elements reproducing the corresponding elements of the simulated circuit: each element is described by symbolic relationship that is internally solved by the software to produce an efficient, optimized code.

Authors have analyzed different scenarios in which the secondary coil is optimized with respect to different values of load R_L.

In order to check sensitivity of performed optimization, simulations are performed in perturbed/off design conditions: multiple simulations are performed considering perturbed/tolerated values of the applied load R_{Ltol} with respect to its design value R_L.

In this way, authors want to verify how a compensation designed for a value of R_L different from R_{opt} is robust with respect to a tolerated load R_{Ltol}.

Different simulated conditions are shown in Table 6.

Simulation results in terms of efficiency and transferred power are shown in Figures 15 and 16: with a proper tuning of L_{f2}, C_{2*}, and C_{f2}, system can be designed for a wide range of different load resistances R_L with limited consequences on efficiency.

Also if the load is different from its design value (R_L different from R_{opt}), performance sensitivity is quite low.

Power transfer can be modulated with limited consequences on system efficiency.

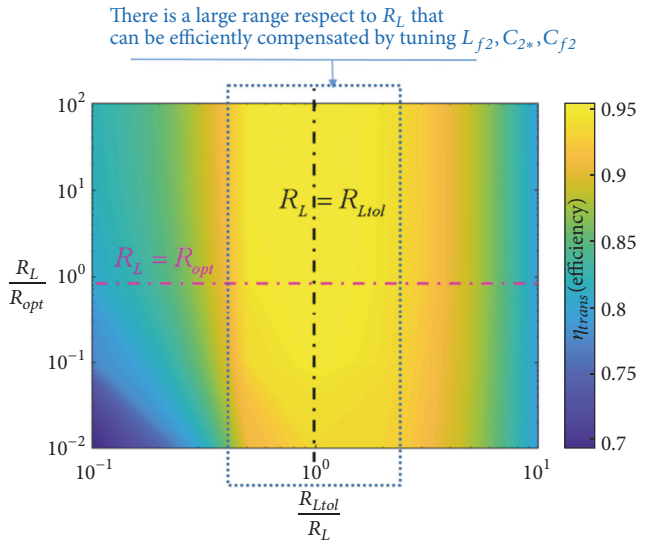

Figure 15: LCC compensation, behavior of power transfer efficiency with respect to R_L / R_{opt} and R_{Ltol}/ R_{opt}.

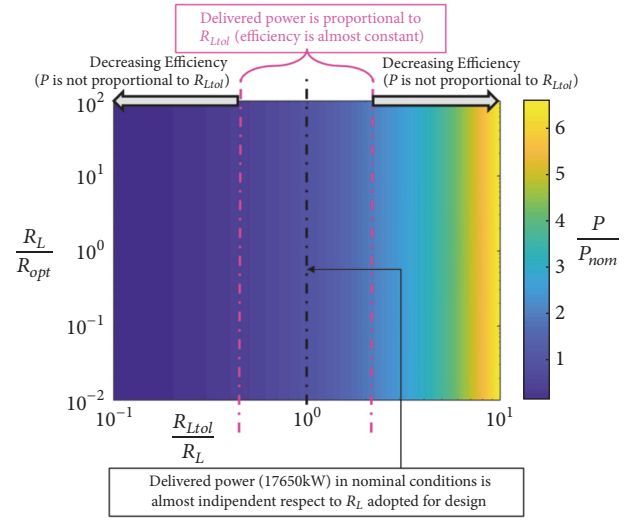

Figure 16: LCC compensation, behavior of power transfer P with respect to its nominal design value P_{nom}.

As in the case of series-series topology, efficiency is almost constant with respect to a power transfer modulation between 15 and 30 kW. Obtained efficiencies are only a bit lower with respect to series-series compensation. This

Table 6: Parameters of the simulated circuit with LCC compensation.

Design Load for the compensation of the secondary Pad	Simulated load values (R_{Ltol}) *(0.1Nom.)Min*//half//Nominal//double//**Max10Nom)**
0.153[Ω](0.01 R_{opt})	*0.0153*// 0.0765// 0.153//0.306// **1.53** [Ω]
1.53[Ω](0.1 R_{opt})	*0.153*// 0.765// 1.53//3.06// **15.3** [Ω]
15.3[Ω](R_{opt})	*1.53*// 7.65// 15.3//30.6// **153** [Ω]
153[Ω](10R_{opt})	*15.3*// 76.5// 153//306// **1530** [Ω]
1530[Ω](100R_{opt})	*153*// 765// 1530//3060// **15300** [Ω]

disadvantage is largely compensated by an easier and more efficient coupling with connected load.

Figure 16 shows the behavior of transferred power scaled with respect to a nominal value of about 17.5 kW with respect to R_L / R_{opt} and R_{Ltol}/ R_{opt}. This power transfer is slightly different with respect to the design value of 15 kW of the series-series one. This slight difference is caused by approximations of design models described in Figure 14 with respect to the full model simulated in Matlab.

Transferred power is approximately proportional to R_{Ltol}/ R_{opt} (around nominal conditions) reproducing a behavior which is quite similar with respect to the one of series-series topology.

6. Conclusions and Further Developments

In this work authors have proposed an innovative application of the wireless power transfer to railway "Parking" functionality (power collection in standstill conditions).

According to performed analysis series-series compensation assures the highest performances in terms of efficiency.

However, LCC topology offers a greater design flexibility.

In series-series topology the resistance has to be carefully tuned to optimize transfer efficiency.

In LCC one, there is an additional resonating branch on the secondary coil which is tuned to improve the power transfer between the secondary coil and the load. Clearly this additional degree of freedom helps to make the system more flexible with respect to load variations.

Preliminary calculations have been performed with cautious specifications (high values of air-gap, low coupling between coils). However, obtained results are quite encouraging. For this reason, authors are quite confident that obtained results are even to be conservative with respect to the potentialities of fully optimized industrial products with less demanding specifications. In particular, a possible reduction of pad size with respect to delivered power for the following reasons is expected:

(i) Better coupling of coils (lower air-gap, more sophisticated coil geometries able to improve magnetic circuit design, and ferromagnetic materials to improve flux guidance).

(ii) Increase of input voltage (transferred power almost depends from the squared value of input voltage).

(iii) Improved cooling (a better or more sophisticated thermal design of the system).

(iv) Advanced power conversion stages for a more flexible control of the whole system; this feature it is very important in order to better adapt recharge functionality to battery SOC[30] (State of Charge) and SOH[31] (State of Health).

All above described improvements will be probably investigated as further developments of this work since authors are managing the assembly of some preliminary prototypes that will be the object of future publications.

Currently authors are focusing their attention on refined FEM analysis for generic coils (not circular; not axial symmetric) with ferromagnetic and shielding materials in order to improve flux guidance. For these activities they are starting from recent publications available in literature [29, 32]. Flux guidance is a quite important topic, also considering consequences arising from possible interaction between dispersed flux and surrounding environment [33].

Another contribution of this work is represented by the application of the electromechanical analogy to the study of resonating circuits. Also in this case proposed methodology has produced original results that should be easily extended and expanded to the study of other topologies.

Adopted Symbols

V_{ac}: Feeding AC voltage of the primary pad

L_1, L_2, M_{12}: Dispersed and mutual inductances of primary and secondary pad

R_1,R_2: Internal resistances of primary and secondary coils

C_1 and C_2: Compensating capacities installed, respectively, on primary and secondary coils

C_{f1}, C_{f2}, L_{f1}, L_{f2}: Added compensating capacities and filters on introduced in LCC compensation

R_L: Equivalent resistance of the load on the secondary coil

k_m: Merit factor, between the pads

η: Total efficiency of the system, obtained as the product of partial efficiencies of different stages

η_{inv}: Efficiency of the primary pad inverter
η_{trans}: Transmission efficiency of both pads
η_{rect}: Rectifier efficiency
$\eta_{DC\text{-}DC}$: Chopper efficiency (final load transfer stage).

Data Availability

There is no data restriction to be applied since all the provided material is an original product of authors. Data used to support the findings of this study are available from the corresponding author upon request.

Conflicts of Interest

The authors declare that they have no conflicts of interest.

References

[1] A. Reatti, F. Corti, L. Pugi et al., "Application of induction power recharge to garbage collection service," in *Proceedings of the 2017 IEEE 3rd International Forum on Research and Technologies for Society and Industry - Innovation to Shape the Future for Society and Industry (RTSI '17)*, pp. 1–5, Modena, Italy, 2017.

[2] P. Albexon, "Bombardier PRIMOVE, catenary-free operation," in *Proceedings of the AusRAIL PLUS '09*, Adelaide, South Australia, 2009.

[3] C. Min, Z. Deng-yan, and X. De-hong, "Contactless Power Supply of Maglev Using Harmonic Injection Method," *Proceedings of the Csee*, 2005.

[4] Y. D. Chung, C. Y. Lee, D. W. Kim, H. Kang, Y. G. Park, and Y. S. Yoon, "Conceptual Design and Operating Characteristics of Multi-Resonance Antennas in the Wireless Power Charging System for Superconducting MAGLEV Train," *IEEE Transactions on Applied Superconductivity*, vol. 27, no. 4, pp. 1–5, 2017.

[5] B. Allotta, L. Pugi, and F. Bartolini, "An active suspension system for railway pantographs: the T2006 prototype," *Journal of Rail and Rapid Transit*, vol. 223, no. 1, pp. 15–29, 2009.

[6] EN 50119 Railway applications, *Fixed Installations - Electric Traction Overhead Contact Lines*, 2nd edition, 2009.

[7] EN 50367 Railway applications, *Current Collection Systems - Technical Criteria for the Interaction between Pantograph and Overhead Line (To Achieve Free Access)*, 2nd edition, 2009.

[8] M. Ceraolo, G. Lutzemberger, E. Meli, L. Pugi, A. Rindi, and G. Pancari, "Energy storage systems to exploit regenerative braking in DC railway systems: Different approaches to improve efficiency of modern high-speed trains," *Journal of Energy Storage*, vol. 16, pp. 269–279, 2018.

[9] G. A. Covic and J. T. Boys, "Modern trends in inductive power transfer for transportation applications," *IEEE Journal of Emerging and Selected Topics in Power Electronics*, vol. 1, no. 1, pp. 28–41, 2013.

[10] S. Y. R. Hui, W. Zhong, and C. K. Lee, "A critical review of recent progress in mid-range wireless power transfer," *IEEE Transactions on Power Electronics*, vol. 29, no. 9, pp. 4500–4511, 2014.

[11] K. A. Kalwar, M. Aamir, and S. Mekhilef, "Inductively coupled power transfer (ICPT) for electric vehicle charging–A review," *Renewable and Sustainable Energy Reviews*, vol. 47, pp. 462–475, 2015.

[12] L. Pugi, A. Reatti, R. A. Mastromauro, and F. Corti, "Modelling of inductive resonant transfer for electric vehicles," *International Journal of Electric and Hybrid Vehicles*, vol. 10, no. 2, p. 131, 2018.

[13] K. Aditya and S. S. Williamson, "Design considerations for loosely coupled inductive power transfer (IPT) system for electric vehicle battery charging-A comprehensive review," in *Proceedings of the Transportation Electrification Conference and Expo (ITEC, '14)*, pp. 1–6, IEEE, 2014.

[14] A. Wheelers, "Inductance Formulas for Circular and Sqaure Coils," *Proceedengs of IEEE*, vol. 70, 1982.

[15] R. P. Wojda and M. K. Kazimierczuk, "Magnetic Field Distribution and Analytical Optimization of Foil Windings Conducting Sinusoidal Current," *IEEE Magnetics Letters*, vol. 4, Article ID 0500204, 2013.

[16] B. Allotta, L. Pugi, A. Reatti, and F. Corti, "Wireless power recharge for underwater robotics," in *Proceedings of the 2017 17th IEEE International Conference on Environment and Electrical Engineering and 2017 1st IEEE Industrial and Commercial Power Systems Europe (EEEIC / I&CPS Europe)*, pp. 1–6, Milan, Italy, 2017.

[17] S. Raju, R. Wu, M. Chan, and C. P. Yue, "Modeling of mutual coupling between planar inductors in wireless power applications," *IEEE Transactions on Power Electronics*, pp. 481–490, 2014.

[18] X. Qu, H. Han, S. C. Wong, K. T. Chi, and W. Chen, "Hybrid IPT topologies with constant current or constant voltage output for battery charging applications," *IEEE Transactions on Power Electronics*, vol. 30, no. 11, pp. 6329–6337, 2015.

[19] W. Li, H. Zhao, J. Deng, S. Li, and C. C. Mi, "Comparison study on SS and double-sided LCC compensation topologies for EV/PHEV wireless chargers," *IEEE Transactions on Vehicular Technology*, vol. 65, no. 6, pp. 4429–4439, 2016.

[20] T. Kan, F. Lu, T. Nguyen, P. P. Mercier, and C. C. Mi, "Integrated Coil Design for EV Wireless Charging Systems Using *LCC* Compensation Topology," *IEEE Transactions on Power Electronics*, vol. 33, no. 11, pp. 9231–9241, 2018.

[21] Z. Yan, B. Song, Y. Zhang, K. H. Zhang, Z. Mao, and Y. Hu, "A Rotation-Free Wireless Power Transfer System with Stable Output Power and Efficiency for Autonomous Underwater Vehicles," *IEEE Transactions on Power Electronics*, 2018.

[22] Y. Yao, Y. Wang, X. Liu, H. Cheng, M. Liu, and D. Xu, "Analysis, Design and Implementation of a Wireless Power and Data Transmission System Using Capacitive Coupling and Double-sided LCC Compensation Topology," *IEEE Transactions on Industry Applications*, vol. 55, no. 1, pp. 541–551, 2018.

[23] D. C. Karnopp, D. L. Margolis, and R. C. Rosenberg, *System Dynamics: A Unified Approach*, John Wiley & Sons, 1990.

[24] W. Borutzky, *Bond Graph Methodology*, Springer, 2010.

[25] D. J. Ewins, *Modal Testing: Theory and Practice*, vol. 15, Research Studies Press, Letchworth, UK, 1984.

[26] H. Zhi-Fang and H. E. Jimin, *Modal Analysis*, Butterworth-Heinemann, 2001.

[27] A. A. Shabana, *Theory of Vibration - An Introduction*, Springer, 1996.

[28] L. Yun Wei, "Control and Resonance Damping of Voltage-Source and Current-Source Converters With LC Filters," *IEEE Transactions on Industrial Electronics*, vol. 56, no. 5, pp. 1511–1521, 2009.

[29] F. Castelli-Dezza, M. Mauri, A. Dolara, S. Leva, and M. Longo, "Power pad design and optimization for contactless electric vehicle battery charging system," in *Proceedings of the IEEE International Conference on Environment and Electrical Engineering and 2017 IEEE Industrial and Commercial Power Systems Europe (EEEIC/I&CPS Europe '17)*, pp. 1–6, IEEE, 2017.

[30] E. Locorotondo, L. Pugi, L. Berzi, M. Pierini, and G. Lutzemberger, "Online Identification of Thevenin Equivalent Circuit Model Parameters and Estimation State of Charge of Lithium-Ion Batteries," in *Proceedings of the 2018 IEEE International Conference on Environment and Electrical Engineering and 2018 IEEE Industrial and Commercial Power Systems Europe (EEEIC / I&CPS Europe '18)*, pp. 1–6, Palermo, Italy, 2018.

[31] E. Locorotondo, L. Pugi, L. Berzi, M. Pierini, and A. Pretto, "Online State of Health Estimation of Lithium-Ion Batteries Based on Improved Ampere-Count Method," in *Proceedings of the 2018 IEEE International Conference on Environment and Electrical Engineering and 2018 IEEE Industrial and Commercial Power Systems Europe (EEEIC / I&CPS Europe '18)*, pp. 1–6, Palermo, Italy, June 2018.

[32] M. Longo, D. Zaninelli, F. Viola et al., "Recharge stations: A review," in *Proceedings of the Eleventh International Conference on Ecological Vehicles and Renewable Energies (EVER, '16)*, pp. 1–8, IEEE, 2016.

[33] F. Pellitteri, M. Caruso, V. Castiglia, R. Miceli, C. Spataro, and F. Viola, "Experimental Investigation on Magnetic Field Effects of IPT for Electric Bikes," *Electric Power Components and Systems*, vol. 46, no. 2, pp. 125–134, 2018.